Talanta 250 (2022) 123736

Contents lists available at ScienceDirect

Talanta

journal homepage: www.elsevier.com/locate/talanta

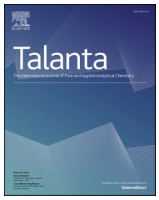

In situ synthesis of ultrafine Cu_2O on layered double hydroxide for electrochemical detection of S-nitrosothiols

Pinghua Ling *, Xinyu Sun, Xianping Gao Pei Yang, Feng Gao **

Laboratory of Functionalized Molecular Solids, Ministry of Education, Anhui Key Laboratory of Chemo/Biosensing, College of Chemistry and Materials Science, Anhui Normal University, Wuhu, 241002, PR China

ARTICLE INFO

Keywords:
S-Nitrosothiols
Electrochemical biosensor
Ultrafine Cu_2O
Layered double hydroxide

ABSTRACT

The identification and quantitation of S-nitrosothiols (RSNO) has aroused enormous levels of attention, due to RSNO have many roles in vivo. Here, we synthesized the nanocomposites of ultrafine Cu_2O/layered double hydroxide (u-Cu_2O/LDH) by the in situ topotactic reduction of a Cu^{2+}-containing LDH with ascorbic acid under gentle conditions and applied these u-Cu_2O/LDH to detect and monitor RSNO. Electrochemical signals of u-Cu_2O/LDH exhibited a wide N-acetyl-S-nitrosopenicillamine detection range from 5.0 nM–4.0 μM and 4.0 μM–400 μM, with a low detection limit of 1.58 nM. The sensor also exhibited good performance for other RSNO, such as S-nitrosoglutathione, S-nitrosocysteine, and S-nitrosohomocysteine with corresponding limits of detection at 1.94 nM, 1.23 nM and 1.62 nM, respectively. The high levels of selectivity and sensitivity to RSNO in complex biological environments can be attributed to the abundance of exposed active sites, and the underlying support structure. In addition, u-Cu_2O/LDH also exhibited dynamic nitric oxide (NO) monitoring ability from living cells. Collectively, these results reveal that u-Cu_2O/LDH exhibit a remarkable ability to quantify RSNO levels in complex samples, and could therefore provide new tools for exploring ultrafine nanomaterials as a potential biosensor to investigate biological events.

1. Introduction

As important nitric oxide (NO) carriers, sinks and reservoirs molecules, S-nitrosothiols (RSNO) usually exist in blood and within living cells and are generated in vivo via the nitrosylation of thiols by oxidative intermediates of endogenous NO [1], which play several functions in regulating a diverse array of physiological functions [2–7]. RSNO can exist in many different forms, including low molecular weight (LMW) RSNO such as S-nitrosoglutathione (GSNO) and S-nitrosocysteine (CySNO) and high molecular weight (HMW) RSNO such as S-nitrosoalbumin (AlbSNO) and S-nitrosohemoglobin (HbSNO) [8,9]. Due to the physiological functions of RSNO often mirror those of NO, RSNO concentrations have been identified as important in a number of disease states, including Parkinson's disease, sepsis, heart failure, asthma, and tuberculosis [3–7,10]. On the other hand, RSNO have low stability and could decompose to release NO via various pathways such as temperature, pH, light irradiation, various reductants and presence of copper ions. Thus, to elucidate the biological roles of RSNO in body, quantify their real-time levels, and investigate their molecular mechanisms, it is vital that we develop effective method to monitor RSNO. The development of electrochemical method for profiling RSNO represents a significant challenge, and the combined application of visible photolysis, enzyme or nanomaterials is generally acknowledged as a common strategy for RSNO detection [11–14]. However, these strategies are unstable and low efficiency and sensitivity, thus significantly reducing their potential application. Thus, it is a real need to develop new strategies or nanomaterials with improved performance for the detection of RSNO.

It is reported that S–NO group in RSNO could decompose rapidly to release NO by metal organic frameworks, transition metal (Cu and Fe) complexes, and nanomaterials [15–21]. However, the high efficiency decomposition of RSNO under physiological pH remains a challenge. Among many nanomaterials, cuprous oxide (Cu_2O) due the low-cost, multielectron transfer properties shows great promise in heterogeneous catalysis [22,23]. Cu_2O with different defined shapes and sizes has previously been prepared and employed to decompose RSNO [24]. The prepared Cu_2O has large size of tens to hundreds of nanometers, which has less surface-active sites, restricting their catalytic

* Corresponding author.
** Corresponding author.
E-mail addresses: phling@ahnu.edu.cn (P. Ling), fgao@mail.ahnu.edu.cn (F. Gao).

https://doi.org/10.1016/j.talanta.2022.123736
Received 27 March 2022; Received in revised form 20 June 2022; Accepted 10 July 2022
Available online 16 July 2022

performance. In order to address the aforementioned challenges, ultrafine nanostructured nanomaterials with lateral size of less than 10 nm offer a promising approach [25,26]. Therefore, designing and preparing ultrafine Cu_2O with improved catalytic activity toward RSNO is urgent.

Layered double hydroxide (LDH) which is a family of two-dimensional layered clays have been extensively studied as catalyst supports or catalyst precursors [27]. Ultrafine Cu_2O could be prepared by the in situ reduction of Cu^{2+} species in Cu^{2+}-containing LDH using mild reducing agents [28,29]. In this process, only Cu^{2+} are reduced, whilst the basic LDH structure could remain. Through this strategy ultrafine and well dispersed Cu_2O could be obtained, which is ascribed to the high dispersity of Cu^{2+} ions in LDH and the large surface of LDH [30,31]. It is important that the formed ultrafine Cu_2O will have good dispersibility and catalytic activity in the aqueous reaction medium used for RSNO decomposition.

Herein, the nanocomposites of ultrafine Cu_2O/LDH (u-Cu_2O/LDH) fabricated by the in situ topotactic reduction of Cu^{2+}-containing LDH with ascorbic acid under gentle conditions, which was acted as electrode material and applied to detect RSNO for the first time (Scheme 1). The formed ultrafine Cu_2O with sub-5 nm could decompose RSNO to generate NO, sequentially the generated NO could be electrocatalytically reduced by Zn^{2+} in the LDH on the electrode [32]. The obtained u-Cu_2O/LDH showed superior selectively and sensitively for the detection of RSNO. Furthermore, these nanocomposites exhibited high performance with regards to the real-time detection of NO released from living cells. All the results implied that the ultrafine Cu_2O and the highly exposed surface site in these nanocomposites allowed the nanocomposites with high performance to detect RSNO in complex sample.

2. Experimental

2.1. Materials and reagents

Zinc chloride ($ZnCl_2$), copper chloride dihydrate ($CuCl_2{\cdot}2H_2O$), *t*-butyl nitrite (90%), glutathione (GSH), L-cysteine (L-Cys), D,L-homocysteine, N-acetyl-S-nitrosopenicillamine (SNAP), Nω-nitro-L-arginine methyl ester hydrochloride (L-NAME), L-arginine (L-Arg) and ascorbic acid were purchased from Sigma Aldrich Inc. (Shanghai, China). Sodium hydroxide (NaOH) and sodium carbonate (Na_2CO_3) were obtained from Pharmaceutical Group Co., Ltd. The aforementioned reagents were all of analytical grade without additional purification. N_2 (99.999%) and NO (99.999%) were obtained from the Xuancheng Sanyuan Gas Co., Ltd. Ultra-pure water (≥18.25 MΩ, Milli-Q, Millipore) was used in all experiments.

2.2. Apparatus

Transmission electron microscopy (TEM) images were obtained on a JEOL JEM-2010 microscope. The scanning electron microscope (SEM) images were carried out on an S-4800 scanning electron microscope (Hitachi, Japan). X-ray photoelectron spectroscopy (XPS) was acquired on an ESCALAB 250Xi spectrometer. Powder X-ray diffraction (XRD) patterns were recorded advance X-ray powder diffractometer operating at 40 kV and 40 mA (CuKα radiation, λ = 1.5418 Å). Fluorescence spectra were measured on an F-7000 spectrometer (HITACHI, Japan). UV–vis absorption spectra were acquired on a Hitachi U-3900 UV/vis spectrometer (Hitachi, Japan). Cyclic voltammetry (CV) and amperometric measurements were carried out on a CHI 660C electrochemical workstation (Shanghai CH Instruments, China) with three electrode system, modified indium tin oxide (ITO) electrode as working electrode, Ag/AgCl as reference electrode and platinum wire as the auxiliary electrode.

2.3. Synthesis of CuZn-LDH nanosheets (denoted herein as LDH nanosheets)

10 mmol $ZnCl_2$, and 10 mmol $CuCl_2{\cdot}2H_2O$ were dissolved in 15 mL ultrapure water, which was as solution A. Solution B was prepared by dissolving NaOH (60 mmol) and Na_2CO_3 (20 mmol) in 15 mL ultrapure water. Next, solution A and solution B were simultaneously added dropwise into 15 mL of ultrapure water at room temperature and pressure under vigorous stirring to form a blue slurry, and then heated at 60 °C under continuous magnetic stirring for 16 h. After centrifugating and washing several times with ultrapure water, the LDH nanosheets was obtained. The obtained LDH was dried at 60 °C for 12 h, and then for subsequent use.

2.4. Synthesis of u-Cu_2O/LDH

50 mL LDH suspension (2 mg/mL) was added dropwise into 50 mL ascorbic acid solution (0.5 M, pH ≈ 9) and stirred for a period of time t (where t = 1, 2 and 3 h) at room temperature and pressure. The products were obtained by centrifugating and washing with ultra-pure water for several times, and dried at 60 °C for 12 h. The obtained samples are denoted herein as u-Cu_2O/LDH-1, u-Cu_2O/LDH-2 (also termed u-Cu_2O/LDH), u-Cu_2O/LDH-3, respectively.

2.5. Synthesis of RSNO

The RSNO were prepared using a simple method [33]. For S-nitrosoglutathione (GSNO), in brief, 0.1 mmol glutathione (GSH) was added into 1.0 mL ice-cold H_2O, then 12 μL *t*-butyl nitrite (0.1 mmol) was added. After 30 min, the deep red solution, GSNO, was obtained.

In the case of S-nitrosocysteine (CysNO), and S-nitrosohomocysteine (HCysNO), the procedure was same to the synthesis of GSNO, except that the 0.1 mmol GSH is replaced by 0.1 mmol L-cysteine and 0.1 mmoL D,L-homocysteine, respectively.

All RSNO solutions were prepared prior to use. The concentrations of the RSNO solutions were monitored by UV–vis spectroscopy (maxCysNO = 337 nm, $\varepsilon = 900\ M^{-1}\ cm^{-1}$ [33], maxGSNO = 335 nm, $\varepsilon = 922\ M^{-1}\ cm^{-1}$ [34], maxHCysNO = 335 nm, $\varepsilon = 606\ M^{-1}\ cm^{-1}$ [7], and

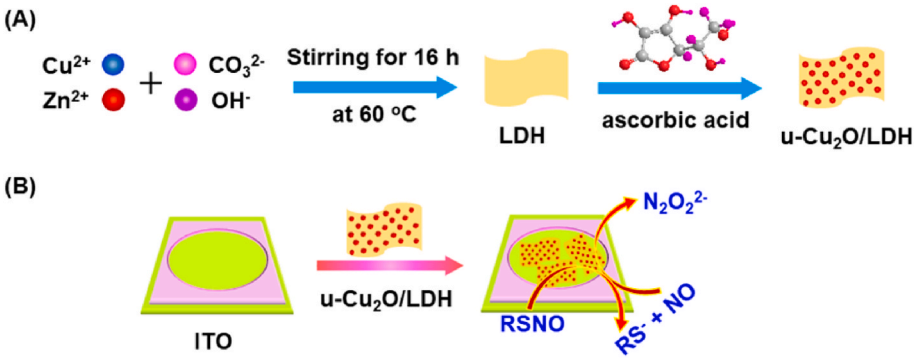

Scheme 1. Schematic Illustration of (A) Synthesis of u-Cu_2O/LDH and (B) Electrochemical Detection Strategy for RSNO.

maxSNAP = 335 nm, $\varepsilon = 519\ M^{-1}\ cm^{-1}$ [7]).

2.6. Preparation of NO in solution

Firstly, 10 mL phosphate buffer solution (PBS, pH = 7.4) was bubbled with high purity nitrogen for 30 min to remove oxygen. Then pure NO was charged for 30 min. The saturated NO solution (1.8 mM at 20 °C [35]) was obtained. Standards were freshly made for each experiment and stored at 0 °C. Different concentrations of NO standard solution were prepared by diluting the saturated solution using

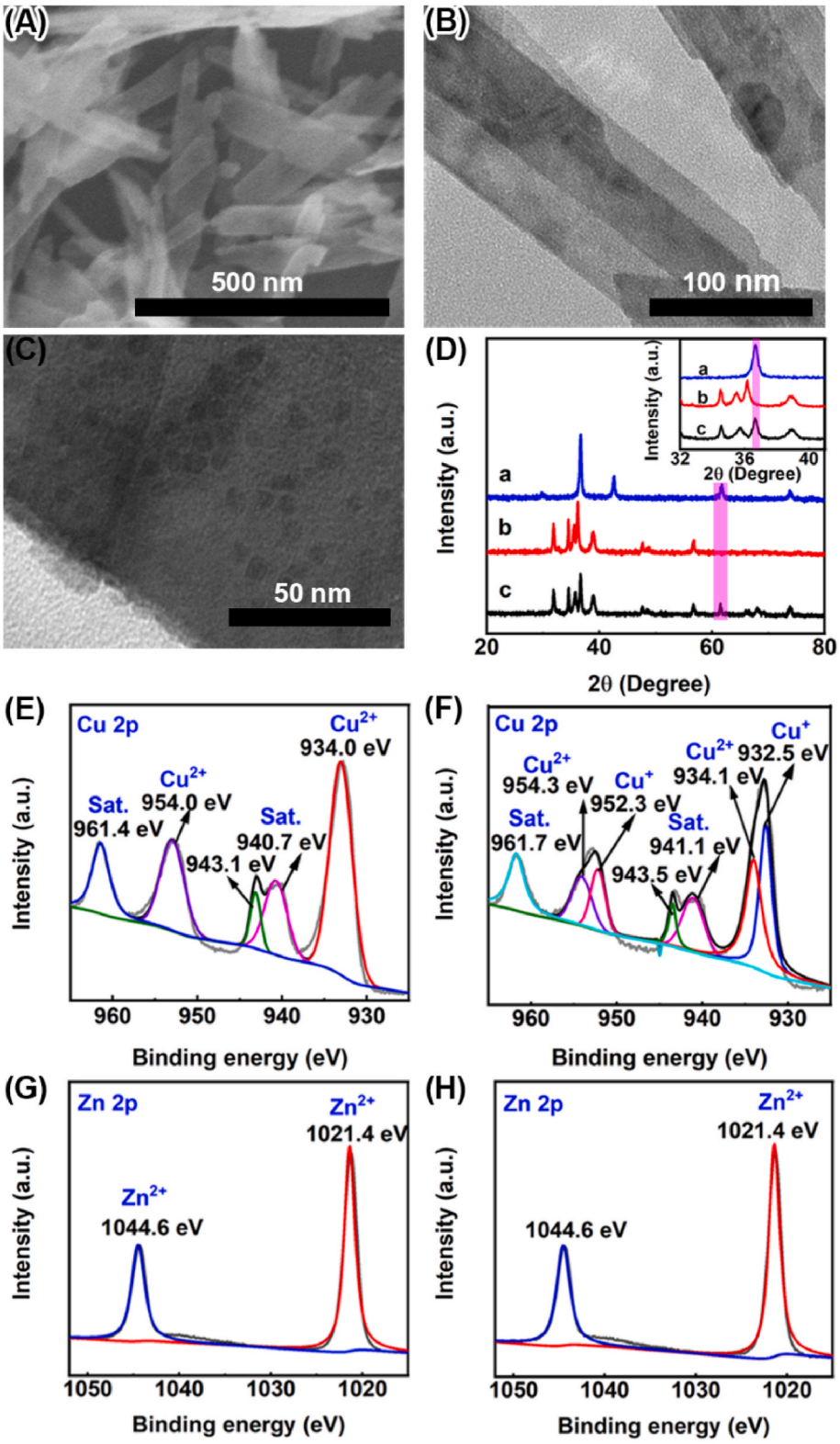

Fig. 1. (A) SEM and (B)TEM images of LDH, (C) TEM images of u-Cu_2O/LDH, (D) XRD patterns (inset XRD pattern from 2θ = 32 - 42°) for Cu_2O (a), LDH (b) and u-Cu_2O/LDH (c). Cu2p XPS spectrum of (E) LDH and (F) u-Cu_2O/LDH. Zn2p XPS spectrum of (G) LDH and (H) u-Cu_2O/LDH.

deoxygenated PBS.

2.7. Cell culture

HeLa cell (Human cervix adenocarcinoma), HEpG2 (human liver cancer cells), RAW (macrophage cells), HUVECs (human umbilical vein endothelial cells), and U87 (human glioma cell line) were cultured using Dulbecco's minimal essential (DMEM) medium supplemented with 10% fetal bovine serum (FBS). All the cells were maintained at 37 °C in a humidified atmosphere (95% air and 5% CO_2) and were kept in logarithmic growth.

2.8. Electrochemical detection of RSNO and NO

Prior to the experiment, ITO electrodes (1.0 cm × 2.5 cm) were washed with 1.0 M KOH, acetone, ethanol, and deionized water, each for 15 min, and dried at 120 °C for 2 h. Firstly, 1.0 mg u-Cu_2O/LDH was dispersed in 1.0 mL of water by sonication for 60 min. Then, 10 μL of u-Cu_2O/LDH suspension (1.0 mg/mL) was spread onto the ITO surface. After dried, 10 μL Nafion (0.5%) was cast onto the electrode and air-dried for further use.

For cells detection, cells were seeded on the u-Cu_2O/LDH/ITO electrode at a density of ~2×10^5 cell/cm^2 and cultured for 24 h. During the amperometric test, L-Arg and L-NAME was used as the stimulant for NO releasing and the inhibitor of nitric oxide synthetase (NOS), respectively.

3. Results and discussion

3.1. Synthesis and characterization of u-Cu_2O/LDH

We used ascorbic acid as the reducing agent via a one-step in situ reduction approach to obtain u-Cu_2O/LDH (Scheme 1A). Briefly, $CuCl_2$ and $ZnCl_2$ were mixed with NaOH and Na_2CO_3 solution to form LDH. Subsequently, the ascorbic acid solution was added to induce ultrafine Cu2O formation.

Scanning electron microscope (SEM) (Fig. 1A) and transmission electron microscopy (TEM) (Fig. 1B) showed that LDH was nanosheet with the mean diameter approximately 400 nm. Fig. 1C revealed that the ultrafine Cu_2O particles with an average size of 5 nm was dispersed uniformly on the LDH nanosheets. The X-ray diffraction (XRD) were applied to evaluate the structure of prepared u-Cu_2O/LDH. Compared with Cu_2O (Fig. 1D, curve a) and LDH (Fig. 1D, curve b), two peaks at 36.5° and 61.52° were observed in u-Cu_2O/LDH, which were indexed to Cu_2O (111) facets and Cu_2O (220) facets, respectively, indicating the formed Cu_2O was cubic-phase (JCPDS No. 65–3288) (Fig. 1D, curve c). These results indicated the u-Cu_2O/LDH with the general preservation of the LDH structure had been successfully synthesized via the mild ascorbic acid reduction process.

Furthermore, X-ray photoelectron spectra (XPS) were applied to evaluate the chemical composition of prepared u-Cu_2O/LDH. By fitting the XPS spectrum of Cu2p of LDH (Fig. 1E), two strong binding energy peaks at 934.0 eV and 954.0 eV were observed, which are assigned to the Cu 2p3/2 and Cu 2p1/2 peaks of the Cu^{2+}, respectively [36,37], indicating the chemical state of Cu in LDH is Cu^{2+}. After LDH reacted with ascorbic acid (Fig. 1F), two peaks at binding energies of 932.5 eV and 952.3 eV appeared, which are assigned to Cu 2p3/2 and Cu 2p1/2 peaks of the Cu_2O, respectively, showing the Cu^+ formed in the reduction process [38–40]. In addition, the chemical state of Zn in LDH before and after reacting with ascorbic acid was also investigated (Fig. 1G and H). The deconvoluted XPS spectrum for Zn in LDH with two peaks located at 1044.6 eV and 1021.4 eV were observed, which are indexed to Zn 2p1/2 and Zn 2p3/2 of Zn^{2+}, respectively (Fig. 1G) [32]. After LDH reacted with ascorbic acid, the XPS result of Zn was similar to that before reacting, revealing Zn in LDH was the form of Zn^{2+} and was not affected by ascorbic acid. These results confirmed that u-Cu_2O/LDH had been successfully synthesized via a gentle reaction method.

In order to explore the evolution of ultrafine Cu_2O during the in situ reduction process, the effects of ascorbic acid reduction time were studied by XRD and TEM. As shown in Fig. S1A, the XRD patterns for u-Cu_2O/LDH showed that the intensity of Cu_2O (111) and Cu_2O (220) diffraction peak increased with ascorbic acid reduction time from 1 h to 3 h, suggesting the formation and growth of ultrafine Cu_2O. On the other hand, no noticeable change was observed between the reaction time of 2 h and 3 h from the XRD result, showing the formation and growth of ultrafine Cu_2O were completed within 2 h. TEM images were used to study the morphological evolution of ultrafine (Figs. S1B–D). The results showed the yield of ultrafine Cu_2O increased with the reaction time increasing and approached a maximum after 2 h, which was consistant with the result of XRD. These results implied that ultrafine Cu_2O with a sub-5 nm of particle size could form on the surface of LDH, whilst maintaining the LDH laminate structure.

3.2. Reactions of u-Cu_2O/LDH to RSNO

To ascertain the catalytic activity of u-Cu_2O/LDH for the denitrosylation of RSNO, fluorescence (FL) spectroscopic and series of UV–vis kinetics curve measurements were studied. To study this process, DAF-FM DA which is a NO-sensitive fluorescent probe was employed. As shown in Fig. 2A, u-Cu_2O/LDH (curve a) and SNAP (curve b) have no peak intensity at 515 nm. When u-Cu2O/LDH was mixed with DAF-FM DA, no peak at 515 nm was observed (curve c). After SNAP was immersed in DAF-FM DA for 60 min (curve d), weak fluorescence intensity was obtained, indicating SNAP was decomposed and NO generated. When LDH was mixed with SNAP and DAF-FM DA for 20 min (curve e), the observed fluorescence intensity was weak, indicating Cu^{2+} and Zn^{2+} has no catalytic activity toward SNAP [32]. Compared with u-Cu_2O/LDH-1 (curve f), the fluorescence intensity was significant increase after u-Cu_2O/LDH immersed in SNAP for 20 min (curve g), indicating an outstanding catalytic activity ultrafine Cu_2O. A similar trend was obtained with other S-nitrosothiols - GSNO, CysNO, and HCysNO (Fig. S2). These results indicated that u-Cu_2O/LDH has high activity in the denitrosylation of RSNO. Furthermore, time-dependent UV–vis experiments were performed to study the performance of catalytic activity of u-Cu_2O/LDH to the denitrosylation of RSNO. A range of RSNO concentrations were employed to test typical Michaelis−Menten curves and fitted by the Lineweaver−Burk equation (Fig. 2B and C and Figs. S3–S5). Some important kinetic parameters such as Michaelis–Menten constant (K_m) and maximum initial velocity (V_{max}) were estimated and listed in Table S1. The apparent K_m of SNAP, CysNO, GSNO, and HCysMO was 1.80 mM, 1.67 mM, 1.93 mM, and 3.60 mM, respectively. K_m value of u-Cu_2O/LDH with CysNO as the substrate was significantly lower than that of other RSNO, showing the u-Cu_2O/LDH has better affinity to CysNO than other RSNO, which may be attributed to the shorter chain length and small size of CysNO compared to other RSNO, leading to good accessibility of CysNO to the active sites of Cu_2O [41]. The apparent K_m of HCysNO was higher than that of other RSNO, which is ascribed to the long chain length of HCysNO that tends to form an unfavorable 7 membered ring as the intermediate [42], so HCysNO has the biggest K_m among these RSNO. These results showed that the high surface area and the exposed activity sits in u-Cu_2O/LDH lead to the high performance of u-Cu_2O/LDH.

3.3. Feasibility of the sensor

In order to investigate the feasibility of the sensor in response to RSNO, we selected SNAP as a model via cyclic voltammetry (CV). Unexpectedly, after different concentrations of SNAP addition, LDH/ITO electrode showed no obvious current peak at around −0.55 V, which is attributed to little NO formed in this process (Fig. 3A). However, upon the addition of the different concentrations of SNAP, the u-Cu_2O/LDH demonstrated the strong electrochemical signal which was increased

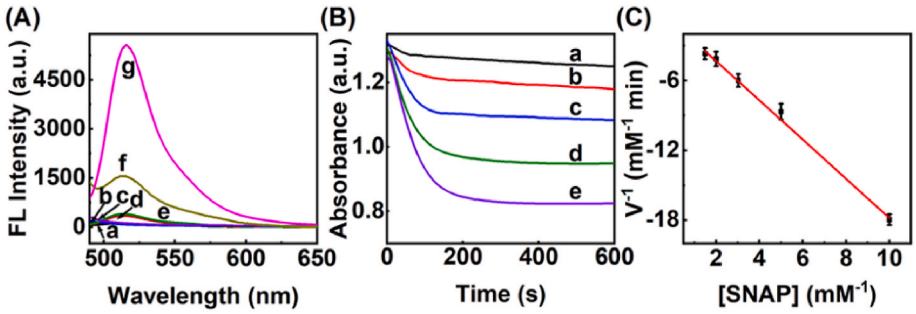

Fig. 2. (A) Fluorescence spectra of u-Cu_2O/LDH (a), SNAP (b), u-Cu_2O/LDH + DAF-FM DA (c), SNAP + DAF-FM DA (d), LDH + SNAP + DAF-FM DA (e) u-Cu_2O/LDH-1 + SNAP + DAF-FM DA (f) and u-Cu_2O/LDH + SNAP + DAF-FM DA (g). (Ex = 480 nm). (B)Time-dependent absorbance spectra and (C) The decomposition rates of SNAP with different concentrations: 0.1 mM (a) 0.2 mM (b), 0.33 mM (c), 0.5 mM (c) and 0.67 mM (d) in the presence of 33 μg mL^{-1} u-Cu_2O/LDH.

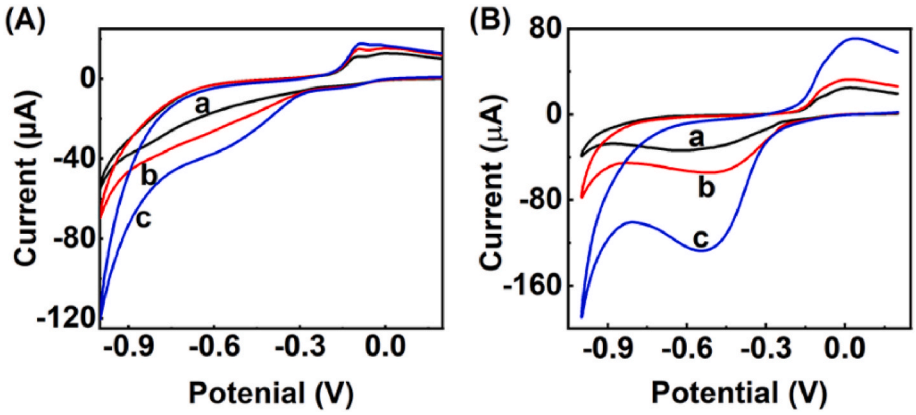

Fig. 3. CV curves of (A) LDH/ITO in a 0.1 M PBS solution containing 0 μM (a), 10 μM (b) and 90 μM (c) SNAP. (B) u-Cu_2O/LDH/ITO in a 0.1 M PBS solution containing 0 μM (a), 30 μM (b) and 70 μM (c) SNAP.

with the increasing SNAP concentration (Fig. 3B). This phenomenon can be described due to the SNAP was decomposed by ultrafine Cu_2O on the surface of LDH, and thus, NO was released, resulting in the detectable electrochemical signal. To identify the principle behind this process, the LDH and u-Cu_2O/LDH modified electrodes were employed to detect NO and results were shown in Fig. S6. The results showed that the similar peak current at −0.55 V was obtained in the presence of the same concentration of NO, suggesting that the formed ultrafine Cu_2O did not affect the electrocatalytic properties of LDH toward NO. Furthermore, the XPS spectrum of u-Cu_2O/LDH was recorded after reacting with SNAP (Fig. S7). This allowed us to identify two binding energy peaks at 932.6 eV (Cu^+ 2p3/2) and 933.9 eV (Cu^{2+} 2p3/2), thus exhibiting a higher molar ratio of Cu^{2+} to Cu^+ compared to that before reacting with SANP (Fig. 1F). Thus, it could be verified that Cu^+ on the surface of LDH was oxidized into Cu^{2+} by SNAP and NO released. And then the formed NO was reduced and detected on the LDH/ITO electrode.

3.4. Detection of RSNO

Fig. 4A depicted the amperometric record for u-Cu_2O/LDH in 0.1 M PBS with different concentrations of SNAP. The peak current increased with the SNAP concentration increasing. As shown in Fig. 4B, the peak currents exhibited a good proportion to the logarithm of SNAP concentration with two linear ranges of 5.0 nM to 4.0 μM and 4.0 μM–400 μM. The limit of detection (LOD) for SNAP was 1.58 nM at the S/N = 3, which was lower than that of the method of glutathione peroxidase-

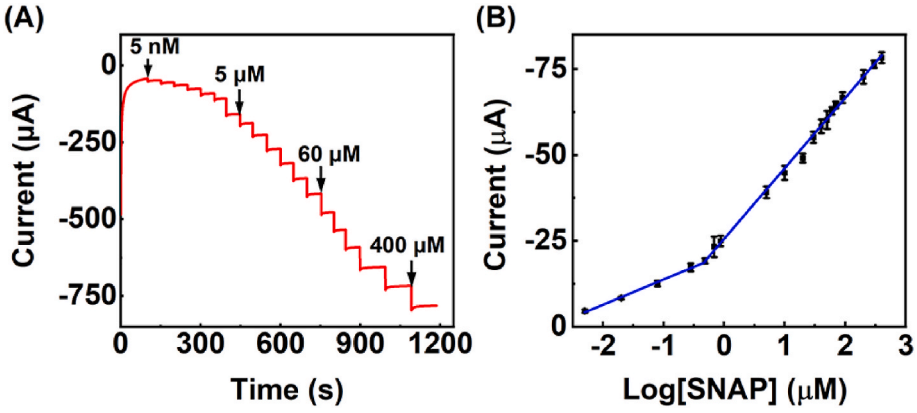

Fig. 4. (A) Amperometric response and (B) Linear calibration curve between logarithm of current and logarithm of SNAP concentration.

based amperometric biosensor (400 nM) [12]. In addition to SNAP, other RSNO such as CysNO, GSNO and HCysNO was tested. As shown in Figs. S8–S10, u-Cu_2O/LDH/ITO displayed excellent current signal response to different RSNO concentration. For CysNO, the LOD was 1.23 nM with two linear ranges of 4.0 nM–4.0 μM and 4.0 μM − 300 μM, which was lower than that of the method based on visible photolysis and amperometric detection of RSNO (40 nM) [43], glutathione peroxidase-based amperometric biosensor (200 nM) [12] and S-Nitrosothiol detection in a microfluidic device (240 nM) [11]. For GSNO, the two linear range is 6.0 nM to 6.0 μM and 6.0 μM–372 μM with LOD of 1.94 nM which was lower than 30 nM and 400 nM of the method based on visible photolysis and amperometric detection [43], and microfluidic method [11], respectively. For HCysNO, the two linear response was from 5.0 nM to 5.0 μM and 5.0 μM–400 μM with the low detection limit of 1.62 nM which was lower than 80 nM of the method based on chromatography coupled with chemical vapor generation atomic fluorescence detection [44]. These results demonstrated that the presence of u-Cu_2O/LDH can provide high sensitivity for RSNO determination at physiologically relevant levels (nM−μM).

3.5. Selectivity, reproducibility, and stability of the biosensor

Selectivity is an important analytical factor for the sensor. Thus, some biological interfering species such as glucose (Glc), dopamine (DA), L-argine (L-Arg), ascorbic acid (AA), H_2O_2, $CuCl_2$ (Cu^{2+}), $ZnCl_2$ (Zn^{2+}), $CaCl_2$ (Ca^{2+}), $FeSO_4$ (Fe^{2+}), $AgNO_3$ (Ag^{+}), $ZrCl_4$ (Zr^{4+}), Ni $(NO_3)_2$ (Ni^{2+}), $Co(NO_3)_2$ (Co^{2+}), $HgCl_2$ (Hg^{2+}), $MnCl_2$ (Mn^{2+}), $NaNO_2$, serotonin and uric acid (UA) with the concentration at 2.0 μM were tested. Fig. S11 depicted that the current response for SNAP (0.3 μM) was remarkably larger than that for these interfering species, demonstrating the sensor has the satisfactory selectivity. The excellent specificity can be attributed to the high catalytic activity of ultrafine Cu_2O toward the denitrosylation of SNAP and the exposed and dispersed uniformly Zn^{2+} in LDH.

In order to estimate the reproducibility, 10 μM SNAP was tested by ten independently u-Cu_2O/LDH/ITO electrodes. The relative standard deviation (RSD) (n = 3) of 1.33% was obtained. For repeatability, the RSD of 1.20% was obtained with ten measurements in response to 10 μM SNAP. After the u-Cu_2O/LDH/ITO electrodes were stored at 4 °C for 21 days, the current still retained about 87.85% of its initial response value (Fig. S12). Thus, the biosensor has satisfactory reproducibility, repeatability and stability. In order to evaluate the practicability of the sensor, serum sample was tested (Fig. S13). Compared to the current response in PBS, the current response in serum was slightly lower, indicating the sensor could be used to detect RSNO in real sample.

3.6. Detection of NO and real-time measurement of NO molecules released from living cells

The electrocatalytic activity of u-Cu_2O/LDH toward NO was also investigated. As shown in Fig. 5A, the reduction current response was increased with the successive addition of NO from 5.0 nM to 500 μM. Fig. 5B shows the peak current exhibited two segments of linear relationships to the logarithm of NO concentration in the range from 5.0 nM to 10 μM and 10 μM–500 μM, respectively. The detection limit of 1.1 nM is calculated at a signal-to-noise ratio of 3, which was lower than 180 nM of the method based on iron phthalocyanine decorated nitrogen-doped graphene as electrode material [45]. 1.3 μM of metal–organic framework modified electrode [46], and 900 nM of poly(TTBA + rGO)/ZnO modified electrode [32]. This excellent analytical performance could be ascribed to the exposed and dispersed uniformly Zn^{2+} active sites in LDH.

Chronoamperometry was used to monitor NO released from Human umbilical vein endothelial cells (HUVECs). The NO release from cell via the addition of L-Arg which is a substrate for nitric oxide synthase (NOS) in biological systems. In order to inhibit the generation of NO, the L-NAME was used. As displayed in Fig. S14A, the bare ITO electrode exhibited no current response in the absence of HUVECs (curve a). When 10 mM L-NAME (curve b) was injected, the u-Cu_2O/LDH/ITO electrode showed no obvious current response. When 10 mM L-Arg (curve c) was injected, the u-Cu_2O/LDH/ITO electrode showed obvious current response, indicating the NO released from HUVECs. While the u-Cu_2O/LDH/ITO electrode displayed obvious decrease current response in the mixture of 10 mM L-Arg and 10 mM L-NAME (curve d), which should be attributed to the specific inhibiting behavior of L-NAME toward NO release. To investigate the performance of the u-Cu_2O/LDH/ITO electrode toward different concentrations of L-Arg was carried out in PBS (Fig. S14B). The result displayed that the NO releases from HUVECs also depend on drug-concentration.

To demonstrate the general performance of this method for NO detection, other cancer cell lines such as U87, HeLa, HEpG2 and RAW lines were tested (Fig. S15). As expected, all of these cell lines showed positive current response. According to the peak current, the order of NO concentration released from cancer cells is ordered in the decreasing sequence: HUVECs > HEpG2 > U87 > RAW > HeLa. These results indicated this is a general method for NO detection.

4. Conclusion

In summary, we fabricated LDH supported ultrafine Cu_2O (u-Cu_2O/LDH) for ultrasensitive RSNO detection and real-time monitoring NO released from living cells. u-Cu_2O/LDH can be synthesized gently with ascorbic acid at room temperature, and possess high activity for the denitrosylation of RSNO, Noticeably, u-Cu_2O/LDH were demonstrated

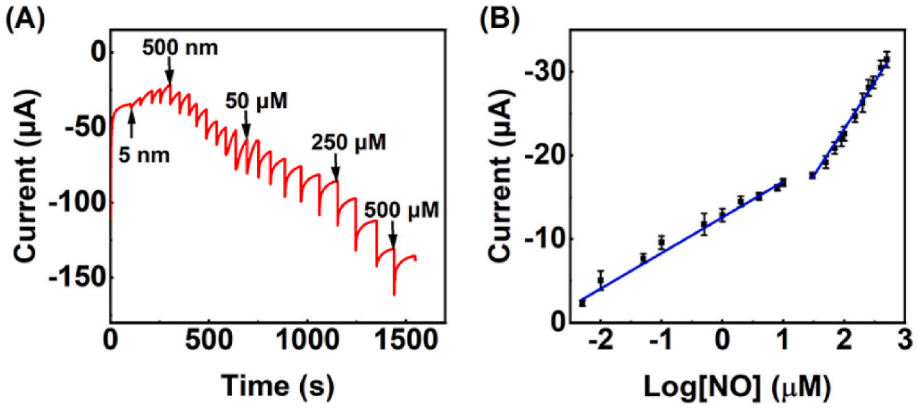

Fig. 5. (A) Amperometric response and (B) Linear calibration curve between logarithm of current and logarithm of NO concentration.

to exhibit reliable stability, high biocompatibility, and fine sensitivity and selectivity for RSNO and NO quantification, due to the ultrafine Cu_2O with highly exposed surface sites and the exposed active sits of LDH. Take advantage of these advantages, u-Cu_2O/LDH can be used for the real-time monitoring of RSNO signaling events in biological systems as high performance tool in future research, and can provide significant insight for creating the high performance ultrafine Cu_2O-based nanomaterials for the bioapplication.

Author statement

P.H. Ling and F. Gao: Funding acquisition, Writing -review & editing the manuscript, planning the projects and designing the experiment X.Y Sun: Data curation and performing the experiments. X.P. Gao, and P. Yang: investigation, and Validation. P.H. Ling and F. Gao supervised and coordinated all investigators for this project. All authors discussed the results and commented on the manuscript.

Declaration of competing interest

The authors declare that they have no known competing financial interests or personal relationships that could have appeared to influence the work reported in this paper.

Acknowledgements

This work was financially supported by the National Natural Science Foundation of China (22074002, 21705004, 21874001).

Appendix A. Supplementary data

Supplementary data to this article can be found online at https://doi.org/10.1016/j.talanta.2022.123736.

References

[1] D.A. Wink, R.W. Nims, J.F. Darbyshire, D. Christodoulou, I. Hanbauer, G.W. Cox, F. Laval, J. Laval, J.A. Cook, M.C.M.C. Krishna, W.G. DeGraff, J.B. Mitchell, Reaction kinetics for nitrosation of cysteine and glutathione in aerobic nitric oxide solutions at neutral pH. Insights into the fate and physiological effects of intermediates generated in the NO/O_2 reaction, Chem. Res. Toxicol. 7 (1994) 519–525.

[2] R. Vercelino, T.M. Cunha, E.S. Ferreira, F.Q. Cunha, S.H. Ferreira, M.G. de Oliveira, Skin vasodilation and analgesic effect of a topical nitric oxide-releasing hydrogel, J. Mater. Sci. Mater. Med. 24 (2013) 2157–2169.

[3] G.F. de Souza, J.K. Yokoyama-Yasunaka, A.B. Seabra, D.C. Miguel, M.G. de Oliveira, S.R. Uliana, Leishmanicidal activity of primary S-nitrosothiols against Leishmania major and Leishmania amazonensis: implications for the treatment of cutaneous leishmaniasis, Nitric Oxide 15 (2006) 209–216.

[4] R. Sengupta, A. Holmgren, Thioredoxin and thioredoxin reductase in relation to reversible S-nitrosylation, Antioxidants Redox Signal. 18 (2013) 259–269.

[5] M. Benhar, M.T. Forrester, J.S. Stamler, Protein denitrosylation: enzymatic mechanisms and cellular functions, Nat. Rev. Mol. Cell Biol. 10 (2009) 721–732.

[6] S. Yuan, R.P. Patel, C.G. Kevil, Working with nitric oxide and hydrogen sulfide in biological systems, Am. J. Physiol. Lung Cell Mol. Physiol. 308 (2015) L403–L415.

[7] P. Anand, J.S. Stamler, Enzymatic mechanisms regulating protein S-nitrosylation: implications in health and disease, J. Mol. Med. 90 (2012) 233–244.

[8] J.S. Stamler, D.I. Simon, J.A. Osborne, M.E. Mullins, O. Jaraki, T. Michel, D. J. Singel, J. Loscalzo, S-nitrosylation of proteins with nitric oxide: synthesis and characterization of biologically active compounds, Proc. Natl. Acad. Sci. U. S. A 89 (1992) 444–448.

[9] D. Giustarini, A. Milzani, I. Dalle-Donne, R. Rossi, Detection of S-nitrosothiols in biological fluids: a comparison among the most widely applied methodologies, J. Chromatogr. B 851 (2007) 124–139.

[10] A. Doctor, R. Platt, M.L. Sheram, A. Eischeid, T. McMahon, T. Maxey, J. Doherty, M. Axelrod, J. Kline, M. Gurka, A. Gow, B. Gaston, Hemoglobin conformation couples erythrocyte S-nitrosothiol content to O_2 gradients, Proc. Natl. Acad. Sci. U. S. A 102 (2005) 5709–5714.

[11] R.A. Hunter, M.H. Schoenfisch, S-Nitrosothiol analysis via photolysis and amperometric nitric oxide detection in a microfluidic device, Anal. Chem. 87 (2015) 3171–3176.

[12] M. Musameh, N. Moezzi, L.M. Schauman, M.E. Meyerhoff, Glutathione peroxidase-based amperometric biosensor for the detection of S-nitrosothiols, Electroanalysis 18 (2006) 2043–2048.

[13] B. Peng, M.E. Meyerhoff, Reexamination of the direct electrochemical reduction of S-nitrosothiols, Electroanalysis 25 (2013) 914–921.

[14] H. Tu, J. Xue, X. Cao, W. Zhang, L. Jin, A novel electrochemical microsensor for the determination of NO and its application to the study of the NO donor S-nitrosoglutathione, Analyst 125 (2000) 163–167.

[15] B.K. Oh, M.E. Meyerhoff, Spontaneous catalytic generation of nitric oxide from S-nitrosothiols at the surface of polymer films doped with lipophilic copperII complex, J. Am. Chem. Soc. 125 (2003) 9552–9553.

[16] J.L. Harding, M.M. Reynolds, Metal organic frameworks as nitric oxide catalysts, J. Am. Chem. Soc. 134 (2012) 3330–3333.

[17] P. Taladriz-Blanco, V. Pastoriza-Santos, J. Perez-Juste, P. Herves, Controllable nitric oxide release in the presence of gold nanoparticles, Langmuir 29 (2013) 8061–8069.

[18] L. Tan, A. Wan, H. Li, Conjugating S-nitrosothiols with glutathiose stabilized silver sulfide quantum dots for controlled nitric oxide release and near-infrared fluorescence imaging, ACS Appl. Mater. Interfaces 5 (2013) 11163–11171.

[19] C.W. McCarthy, R.J. Guillory 2nd, J. Goldman, M.C. Frost, Transition-metal-mediated release of nitric oxide (NO) from S-nitroso-N-acetyl-d-penicillamine (SNAP): potential applications for endogenous release of NO at the surface of stents via corrosion products, ACS Appl. Mater. Interfaces 8 (2016) 10128–10135.

[20] J. Pant, M.J. Goudie, S.P. Hopkins, E.J. Brisbois, H. Handa, Tunable nitric oxide release from S-nitroso-N-acetylpenicillamine via catalytic copper nanoparticles for biomedical applications, ACS Appl. Mater. Interfaces 9 (2017) 15254–15264.

[21] B. Qu, L. Yuan, J. Li, J. Wang, H. Lv, X. Yang, Selenium-containing polyurethane with elevated catalytic stability for sustained nitric oxide release, J. Mater. Chem. B 7 (2019) 150–156.

[22] S. Paria, O. Reiser, Copper in photocatalysis, ChemCatChem 6 (2014) 2477–2483.

[23] J. Cui, U.J. Gibson, A simple two-step electrodeposition of Cu_2O/ZnO nanopillar solar cells, J. Phys. Chem. C 114 (2010) 6408–6412.

[24] S. Ghosh, P. Roy, S. Prasad, G. Mugesh, Crystal-facet-dependent denitrosylation: modulation of NO release from S-nitrosothiols by Cu_2O polymorphs, Chem. Sci. 10 (2019) 5308–5318.

[25] Y. Sun, S. Gao, F. Lei, C. Xiao, Y. Xie, Ultrathin two-dimensional inorganic materials: new opportunities for solid state nanochemistry, Acc. Chem. Res. 48 (2015) 3–12.

[26] C. Tan, X. Cao, X.J. Wu, Q. He, J. Yang, X. Zhang, J. Chen, W. Zhao, S. Han, G. H. Nam, M. Sindoro, H. Zhang, Recent advances in ultrathin two-dimensional nanomaterials, Chem. Rev. 117 (2017) 6225–6331.

[27] Y. Zhao, X. Jia, G.I.N. Waterhouse, L.Z. Wu, C.H. Tung, D. O'Hare, T. Zhang, Layered double hydroxide nanostructured photocatalysts for renewable energy production, Adv. Energy Mater. 6 (2016).

[28] H. Xu, W. Wang, W. Zhu, Shape evolution and size-controllable synthesis of Cu_2O octahedra and their morphology-dependent photocatalytic properties, J. Phys. Chem. B 110 (2006) 13829–13834.

[29] J. Ma, J. Ding, L. Li, J. Zou, Y. Kong, S. Komarneni, In situ reduction for synthesis of nano-sized Cu_2O particles on MgCuAl-LDH layers for degradation of orange II under visible light, Ceram. Int. 41 (2015) 3191–3196.

[30] G. Fan, F. Li, D.G. Evans, X. Duan, Catalytic applications of layered double hydroxides: recent advances and perspectives, Chem. Soc. Rev. 43 (2014) 7040–7066.

[31] Q. Wang, D. O'Hare, Recent advances in the synthesis and application of layered double hydroxide (LDH) nanosheets, Chem. Rev. 112 (2012) 4124–4155.

[32] M.Y. Kim, M.H. Naveen, N.G. Gurudatt, Y.B. Shim, Detection of nitric oxide from living cells using polymeric zinc organic framework-derived zinc oxide composite with conducting polymer, Small 13 (2017), 1700502.

[33] B. Roy, A. du Moulinet d'Hardemare, M. Fontecave, New thionitrites: synthesis, stability, and nitric oxide generation, J. Org. Chem. 59 (2002) 7019–7026.

[34] T.W. Hart, Some observations concerning the S-nitroso and S-phenylsulphonyl derivatives of L-cysteine and glutathione, Tetrahedron Lett. 26 (1985) 2013–2016.

[35] S.L. Ting, C.X. Guo, K.C. Leong, D.H. Kim, C.M. Li, P. Chen, Gold nanoparticles decorated reduced graphene oxide for detecting the presence and cellular release of nitric oxide, Electrochim. Acta 111 (2013) 441–446.

[36] M. Devaraj, R. Saravanan, R. Deivasigamani, V.K. Gupta, F. Gracia, S. Jayadevan, Fabrication of novel shape Cu and Cu/Cu_2O nanoparticles modified electrode for the determination of dopamine and paracetamol, J. Mol. Liq. 221 (2016) 930–941.

[37] S. Tian, J. Liu, R.E. Cowley, P. Hosseinzadeh, N.M. Marshall, Y. Yu, H. Robinson, M.J. Nilges, N.J. Blackburn, E.I. Solomon, Y. Lu, Reversible S-nitrosylation in an engineered azurin, Nat. Chem. 8 (2016) 670–677.

[38] X. An, K. Li, J. Tang, Cu_2O/reduced graphene oxide composites for the photocatalytic conversion of CO_2, ChemSusChem 7 (2014) 1086–1093.

[39] G. Naresh, P.L. Hsieh, V. Meena, S.K. Lee, Y.H. Chiu, M. Madasu, A.T. Lee, H. Y. Tsai, T.H. Lai, Y.J. Hsu, Y.C. Lo, M.H. Huang, Facet-dependent photocatalytic behaviors of ZnS-decorated Cu_2O polyhedra arising from tunable interfacial band Alignment, ACS Appl. Mater. Interfaces 11 (2019) 3582–3589.

[40] G.Z. Yuan, C.F. Hsia, Z.W. Lin, C. Chiang, Y.W. Chiang, M.H. Huang, Highly facet-dependent photocatalytic properties of Cu_2O crystals established through the formation of Au-decorated Cu_2O heterostructures, Chem. Eur J. 22 (2016) 12548–12556.

[41] J.L. Harding, M.M. Reynolds, Composite materials with embedded metal organic framework catalysts for nitric oxide release from bioavailable S-nitrosothiols, J. Mater. Chem. B 2 (2014) 2530–2536.

[42] S.C. Askew, D.J. Barnett, J. McAninly, D.L.H. Williams, Catalysis by Cu^{2+} of nitric oxide release from S-nitrosothiols (RSNO), J. Chem. Soc. Perkin Transactions 2 (1995).

[43] D.A. Riccio, S.T. Nutz, M.H. Schoenfisch, Visible photolysis and amperometric detection of S-nitrosothiols, Anal. Chem. 84 (2012) 851–856.

[44] E. Bramanti, K. Jacovozzi, L. Dulivo, C. Vecoli, R. Zamboni, Z. Mester, A. Dulivo, Determination of S-nitrosoglutathione and other nitrosothiols by p-hydroxymercurybenzoate derivatization and reverse phase chromatography coupled with chemical vapor generation atomic fluorescence detection, Talanta 77 (2008) 684–694.

[45] H. Xu, C. Liao, Y. Liu, B.C. Ye, B.H. Liu, Iron phthalocyanine decorated nitrogen-doped graphene biosensing platform for real-time detection of nitric oxide released from living cells, Anal. Chem. 90 (2018) 4438–4444.

[46] P.H. Ling, X.N. Zang, C.H. Qian, F. Gao, A metal-organic framework with multienzyme activity as a biosensing platform for real-time electrochemical detection of nitric oxide and hydrogen peroxide, Analyst 146 (2021) 2609–2616.